Drug Targeting of HIV-1 RNA·DNA Hybrid Structures: Thermodynamics of Recognition and Impact on Reverse Transcriptase-Mediated Ribonuclease H Activity and Viral Replication†

Tsai-Kun Li,[‡,§] Christopher M. Barbieri,[‡] Hsin-Chin Lin,[∥] Arnold B. Rabson,[∥,⊥,#,△] Gengcheng Yang,[▽] Yupeng Fan,[▽] Barbara L. Gaffney,[▽] Roger A. Jones,[▽] and Daniel S. Pilch*[,‡,⊥]

Departments of Pharmacology, Molecular Genetics and Microbiology, and Pathology, University of Medicine and Dentistry of New Jersey—Robert Wood Johnson Medical School, 675 Hoes Lane, Piscataway, New Jersey 08854-5635, Department of Microbiology, School of Medicine, National Taiwan University, Taipei, Taiwan, ROC 10018, Center for Advanced Biotechnology and Medicine, Piscataway, New Jersey 08854, The Cancer Institute of New Jersey, New Brunswick, New Jersey 08901, and Department of Chemistry and Chemical Biology, Rutgers—The State University of New Jersey, Piscataway, New Jersey 08854-8087

Received February 5, 2004; Revised Manuscript Received April 27, 2004

ABSTRACT: RNA degradation via the ribonuclease H (RNase H) activity of human immunodeficiency virus type I (HIV-1) reverse transcriptase (RT) is a critical component of the reverse transcription process. In this connection, mutations of RT that inactivate RNase H activity result in noninfectious virus particles. Thus, interfering with the RNase H activity of RT represents a potential vehicle for the inhibition of HIV-1 replication. Here, we demonstrate an approach for inhibiting the RNase H activity of HIV-1 RT by targeting its RNA·DNA hybrid substrates. Specifically, we show that the binding of the 4,5-disubstituted 2-deoxystreptamine aminoglycosides, neomycin, paromomycin, and ribostamycin, to two different chimeric RNA−DNA duplexes, which mimic two distinct intermediates in the reverse transcription process, inhibits specific RT-mediated RNase H cleavage, with this inhibition being competitive in nature. UV melting and isothermal titration calorimetry studies reveal a correlation between the relative binding affinities of the three drugs for each of the chimeric RNA−DNA host duplexes and the relative extents to which the drugs inhibit RT-mediated RNase H cleavage of the duplexes. Significantly, this correlation also extends to the relative efficacies with which the drugs inhibit HIV-1 replication. In the aggregate, our results highlight a potential strategy for AIDS chemotherapy that should not be compromised by the unusual genetic diversity of HIV-1.

Reverse transcription is a critical component of retroviral replication (*1*). This process entails the conversion of the viral RNA genome into double-stranded DNA and is dependent on a virus-encoded enzyme termed reverse transcriptase (RT)[1] (*2*, *3*). The complete conversion of the retroviral RNA genome to double-stranded DNA requires two distinct enzymatic activities of RT, a DNA polymerase activity that can use either RNA or DNA as a template, as well as a ribonuclease H (RNase H) activity, which specifically degrades the RNA portions of RNA·DNA hybrid duplex domains (*4*−*6*). HIV-1 reverse transcription involves four main RNase H processing steps (see Figure 1) (*1*): (i) cleavage of the RNA template following minus-strand strong-stop DNA synthesis, (ii) cleavage of the RNA template 3′ to the polypurine tract (PPT) following minus-strand DNA synthesis, (iii) cleavage of the RNA template 5′ to the PPT following minus-strand DNA synthesis, and (iv) cleavage of the host-encoded tRNA as well as the PPT following plus-strand strong-stop DNA synthesis. Mutational studies have demonstrated that genetic inactivation of the RNase H activity of HIV-1 RT results in noninfectious viral particles, an observation highlighting the essential role that RNase H processing plays in the replication of the virus (*4*, *5*).

The pivotal role that RT plays in the replication of HIV-1 has made this enzyme a key target in AIDS chemotherapies (*2*, *3*). However, the efficacies of RT-directed anti-HIV-1 drugs have been compromised by the hypermutability of the HIV-1 genome, which results in drug-resistant viral strains (*2*). Other therapeutic strategies that have been employed to control HIV-1 replication include the use of viral protease inhibitors as well as inhibitors of viral fusion (*3*, *7*−*10*). Like the RT-directed therapies, these two therapeutic approaches are also limited by the genetic diversity exhibited by HIV-

† This work was supported by grants from the American Cancer Society (RSG-99-153-04-CDD) and the National Institutes of Health (CA097123, GM31483, GM48802, and GM60484).

* To whom correspondence should be addressed. Tel: (732) 235-3352. Fax: (732) 235-4073. E-mail: pilchds@umdnj.edu.

‡ Department of Pharmacology, UMDNJ-RWJMS.

§ National Taiwan University.

∥ Center for Advanced Biotechnology and Medicine.

⊥ The Cancer Institute of New Jersey.

Department of Molecular Genetics and Microbiology, UMDNJ-RWJMS.

△ Department of Pathology, UMDNJ-RWJMS.

▽ Rutgers University.

[1] Abbreviations: HIV-1, human immunodeficiency virus type I; RT, reverse transcriptase; RNase H, ribonuclease H; PPT, polypurine tract; PBS, primer binding site; MOI, multiplicity of infection; MTT, methylthiazoletetrazolium; 2-DOS, 2-deoxystreptamine; RRE, Rev response element; TAR, Tat activating region.

10.1021/bi0497345 CCC: $27.50
Published on Web 07/09/2004

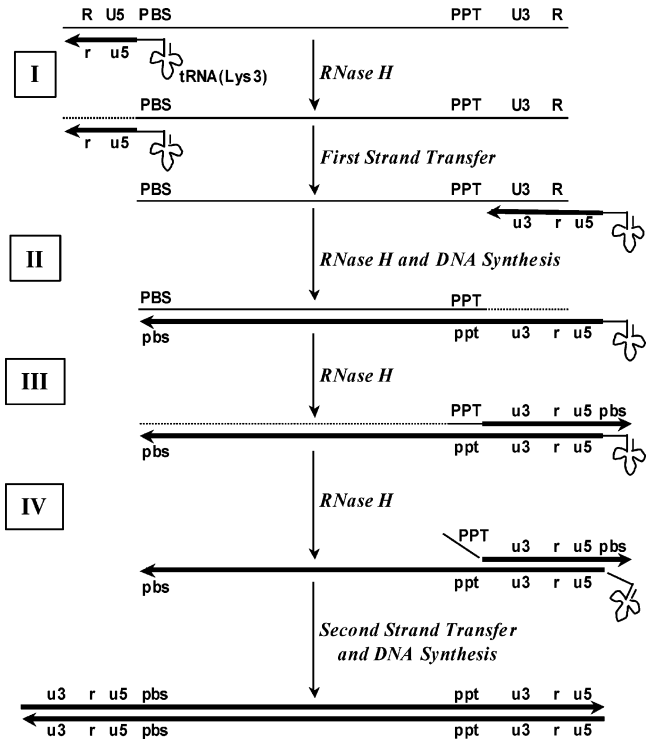

FIGURE 1: (A) Schematic representation of the HIV-1-catalyzed reverse transcription process. In this diagram, DNA strands are depicted as thick lines with arrowheads, while RNA strands are depicted as thin lines. The dashed lines indicate the products of RNase H degradation. The four major RNase H processing steps are denoted by the boxed Roman numerals. PBS denotes the primer binding site, while PPT denotes the polypurine tract.

1, which, in turn, leads to viral protein polymorphism and drug resistance (*3*, *7*). One approach to overcome the problem posed by the unusual genetic diversity of HIV-1 is to target viral components that are not affected by the high mutation frequency associated with the reverse transcription process. In this connection, the RNA·DNA hybrid structures that are formed as intermediates during reverse transcription represent such viral components. These RNA·DNA structures, irrespective of their specific nucleic acid sequence, serve as substrates for the RT-mediated RNase H processing events that are critical to viral replication (*4*, *5*), thereby establishing them as targets for antiretroviral chemotherapy (*11*−*13*).

Aminoglycosides of the 4,5-disubstituted and 4,6-disubstituted 2-deoxystreptamine (2-DOS) classes, which include neomycin, paromomycin, tobramycin, and the kanamycins, preferentially bind A-form relative to B-form nucleic acid structures (*13*−*16*). One of the structural characteristics of RNA·DNA hybrid duplexes is that they adopt A-like conformations (*17*), a feature that makes these duplexes substrates for the binding of 2-DOS aminoglycosides (*12*, *13*, *16*). In this regard, we have shown that the binding of the 2-DOS aminoglycoside, paromomycin, to an octameric RNA·DNA hybrid duplex inhibits the RNA cleaving activities of both calf thymus RNase A and *Escherichia coli* RNase H (*13*). Here, we assess the impact of the 2-DOS aminoglycosides, neomycin, paromomycin, and ribostamycin (see structures in Figure 2), on the RNase H activity of HIV-1 RT as well as on HIV-1 replication. Toward this end, we designed two 18mer oligonucleotide duplexes that mimic two distinct RNA·DNA hybrid structures that serve as RNase H substrates of HIV-1 RT. These duplexes each contain an

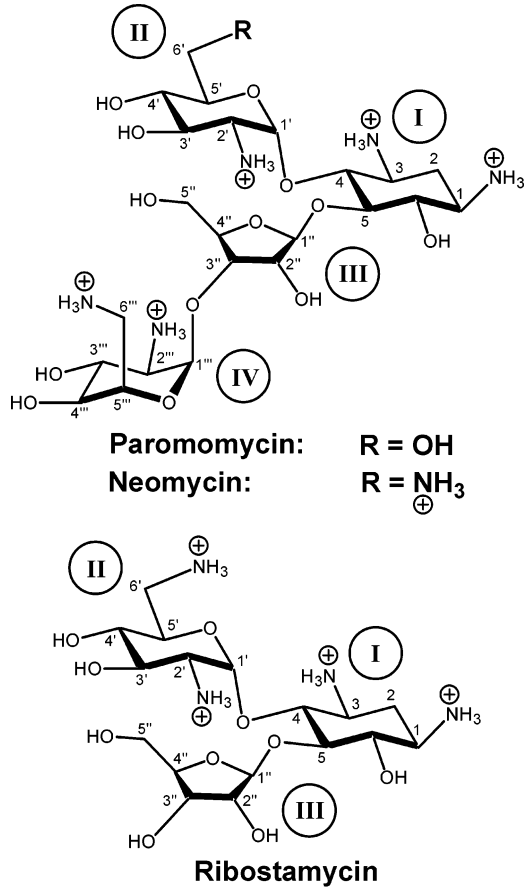

FIGURE 2: Structures of neomycin, paromomycin, and ribostamycin in their fully protonated cationic states, with the atomic and ring numbering systems denoted in Arabic and Roman numerals, respectively.

identical chimeric RNA−DNA strand (18C). One of the two duplexes contains the RNA complement (18R) to the chimeric strand (see Figure 3A), while the other contains the DNA complement (18D) to the chimeric strand (see Figure 3D). The 18C·18R duplex (Figure 3A) mimics the RNase H substrate of HIV-1 RT that follows minus-strand strong-stop synthesis (RNase H processing step I in Figure 1) (*18*), while the 18C·18D duplex (Figure 3D) mimics the RNase H substrate that follows plus-strand strong-stop synthesis (RNase H processing step IV in Figure 1) (*19*). Thus, the 18C·18R and 18C·18D duplexes mimic RNase H substrates that arise at both early and late stages of the reverse transcription process. We demonstrate that the aminoglycosides, neomycin, paromomycin, and ribostamycin, inhibit HIV-1 RT-mediated RNase H cleavage of both the 18C·18D and 18C·18R duplexes as well as HIV-1 replication. Furthermore, the relative extents to which the drugs exhibit these inhibitory effects are correlated with the relative affinities of the drugs for each of the two chimeric duplexes. Our results highlight a strategy for retroviral intervention that will not be compromised by viral genetic diversity.

MATERIALS AND METHODS

Enzyme, Nucleic Acid, and Drug Molecules. Recombinant HIV-1 RT p66, which forms a homodimer that exhibits similar kinetic and equilibrium nucleic acid binding behavior to the p66/p51 heterodimer (*20*), was isolated from *E. coli*

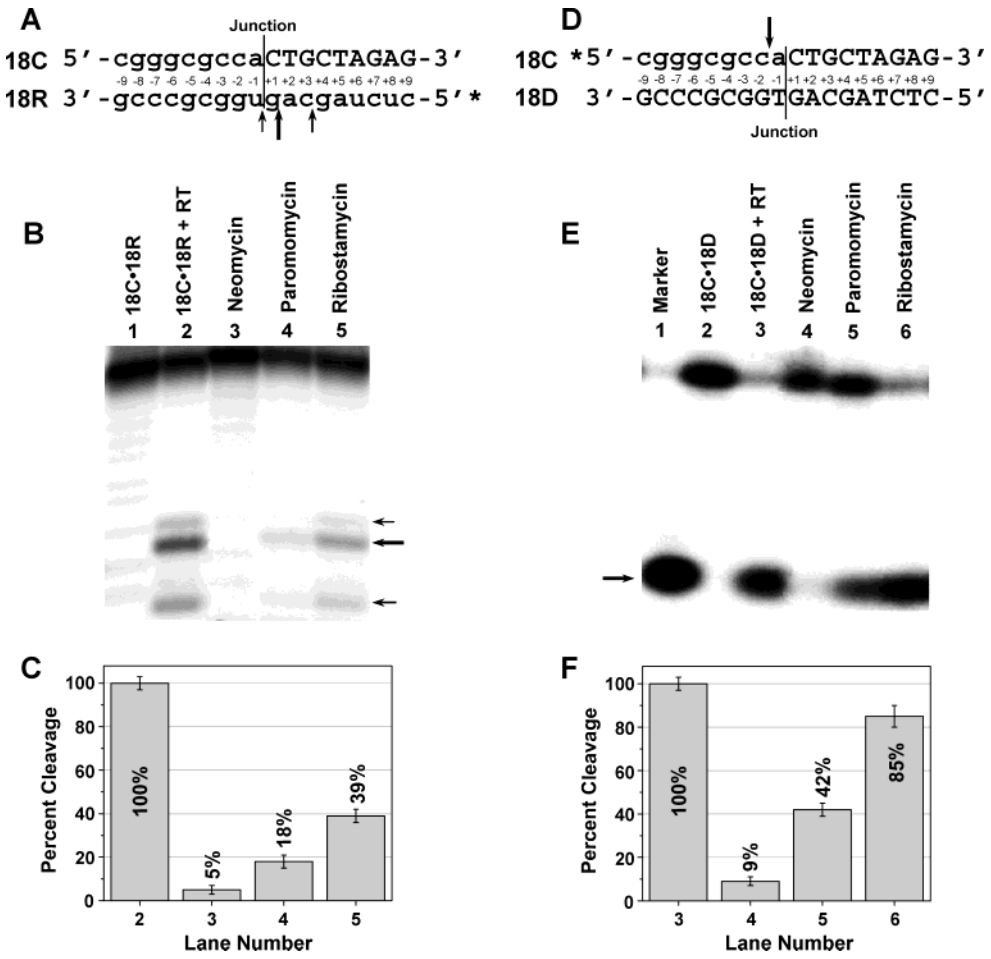

FIGURE 3: Neomycin, paromomycin, and ribostamycin inhibit HIV-1 RT-mediated RNase H cleavage of the 18C·18R and 18C·18D duplexes. (A, D) Schematic representations of the 18C·18R (panel A) and 18C·18D (panel D) duplexes, with the RNA−DNA junction so indicated. RNA bases are presented in lower case, while DNA bases are presented in upper case. The arrows denote the sites of RT-mediated RNase H cleavage, with the relative thickness of the arrows reflecting the relative extents of cleavage. The asterisks denote the sites of the ^{32}P label. (B, E) Denaturing polyacrylamide gels showing RT-mediated RNase H cleavage of the 18C·18R (panel B) and 18C·18D (panel E) duplexes in the absence or presence of the aminoglycosides. The arrows indicate the RNase H cleavage products, which are detailed in the text. In panel B, all of the lanes contain RT except lane 1, with the drug concentration in lanes 3−5 being 62.5 μM. In panel E, all of the lanes contain RT except lanes 1 and 2, with the drug concentration in lanes 4−6 being 2.0 mM. The marker in panel E is a ^{32}P 5′-end-labeled RNA octamer with the sequence 5′-cgggcgcc-3′. (C, F) Quantitation of the extent of RNase H cleavage for the indicated lanes. In panel C, the quantitation corresponds to the primary cleavage site.

JM109 as described previously (*21*). The 18R oligonucleotide was purchased in its PAGE-purified sodium salt form from Dharmacon Research, Inc. (Lafayette, CO). The 18C oligonucleotide was synthesized using phosphoramidites protected as previously described (*22*). The final deprotection and purification strategy used for this chimeric oligonucleotide was described earlier (*23*). The 18D oligonucleotide was synthesized using standard phosphoramidite chemistry and purified by reverse-phase HPLC. The purity of all oligonucleotides was verified by ESI-MS. Neomycin·$3H_2SO_4$·$3H_2O$ and paromomycin·H_2SO_4 were obtained from Fluka, while ribostamycin·$2.5H_2SO_4$·$2H_2O$ was obtained from Sigma. All three drugs were used without further purification.

RNase H Cleavage Assay. The RNase H activity of RT was assayed in a 10 μL reaction mixture containing 10 mM PIPES (pH 6.0) and 5 mM $MgCl_2$. Ten picomoles of either 18C or 18R were ^{32}P-labeled at the 5′ end using T4 polynucleotide kinase. For the cleavage experiments, different aminoglycosides (at concentrations ranging from 0 to 2 mM) were mixed with 0.5 μM target duplex. RT (0.1 μg) was then added to initiate the cleavage reaction. After incubation at 37 °C for 30 min, the reaction was stopped by addition of 3 M urea containing a mixture of bromophenol blue and xylene cyanol. Denaturation of the 18C·18R duplex required the addition of 5 M urea as well as heating at 95 °C for 5 min prior to gel loading. The cleavage products were resolved in a 10% polyacrylamide gel containing 8 M urea. The gels were subsequently analyzed using a phosphoimager (Molecular Dynamics, Inc.).

Circular Dichroism (CD) Spectroscopy. CD measurements were acquired at 25 °C on an Aviv Model 202 spectropolarimeter equipped with a thermoelectrically controlled cell holder. A quartz cell with a 1 cm path length was used for all of the CD studies. CD spectra were acquired from 320 to 215 nm in 1 nm increments, with an averaging time of 2 s. In these studies, nucleic acid concentrations were 5 μM in duplex and solution conditions were 10 mM sodium cacodylate (pH 6.0), 0.1 mM EDTA, and sufficient NaCl to bring the total Na^+ concentration to 25 mM.

Temperature-Dependent Absorption Spectroscopy. All UV absorbance experiments were conducted on an AVIV Model 14DS spectrophotometer (Aviv Biomedical, Inc., Lakewood, NJ) equipped with a thermoelectrically controlled cell holder. A quartz cell with a 1 cm path length was used for all of the

absorbance studies. Absorbance versus temperature profiles were measured at 274 nm with a 5 s averaging time. The temperature was raised in 0.5 °C increments, and the samples were allowed to equilibrate for 1.5 min at each temperature setting. In these thermal denaturation studies, the nucleic acid solutions were 2 μM in duplex and contained aminoglycoside at concentrations ranging from 0 to 10 μM. The buffer solutions for the UV melting experiments contained 10 mM sodium cacodylate (pH 6.0), 0.1 mM EDTA, and sufficient NaCl to bring the total Na^+ concentration to 25 mM. For each optically detected transition, the melting temperature (T_m) was determined as described previously (*24*).

Isothermal Titration Calorimetry (ITC). Isothermal calorimetric measurements were performed at 25 °C on a MicroCal VP-ITC (MicroCal, Inc., Northampton, MA). In a typical experiment, 5 or 10 μL aliquots of aminoglycoside were injected from a 250 μL rotating (300 rpm) syringe into an isothermal sample chamber containing 1.42 mL of a solution containing either 18C·18R or 18C·18D. Each experiment of this type was accompanied by the corresponding control experiment in which the drug was injected into a solution of buffer alone. The duration of each 5 μL injection was 5 s, with the corresponding duration of each 10 μL injection being 10 s. The initial delay prior to the first injection was 60 s. For the ITC titrations of 18C·18R with neomycin and paromomycin, the starting duplex concentration was 10 μM, the starting drug concentration was 350 μM, and the delay between injections was 300 s. In these two titrations, the first injection was 5 μL, with all subsequent injections being 10 μL. For the ITC titration of 18C·18R with ribostamycin, the starting duplex concentration was 100 μM, the starting drug concentration was 3.5 mM, and the delay between injections was 600 s. In this titration, all injections were 5 μL. For the titrations of 18C·18D with neomycin, paromomycin, and ribostamycin, all injections were 5 μL. In the neomycin and paromomycin titrations, the starting 18C·18D concentration was 100 μM in duplex, with the starting drug concentration being 1.75 mM. In the ribostamycin titration, the starting 18C·18D concentration was 500 μM in duplex, while the starting drug concentration was 8.75 mM. The delays between injections in the titrations of 18C·18D with neomycin, paromomycin, and ribostamycin were 240, 600, and 900 s, respectively. The duplex concentration in each of the ITC experiments was chosen such that the unitless product of the primary binding constant (K_1) times the total starting duplex concentration times the primary binding stoichiometry (N_1) fell between 4 and 48, a range well suited for rigorous determination of the binding constant.

Each injection generated a heat burst curve (microcalories per second vs seconds). The area under each heat burst curve was determined by integration [using the Origin version 5.0 software (MicroCal, Inc., Northampton, MA)] to obtain a measure of the heat associated with that injection. The heat associated with each drug−buffer injection was subtracted from the corresponding heat associated with each drug−duplex injection to yield the heat of drug binding for that injection. The resulting corrected injection heats were plotted as a function of the [drug]/[duplex] ratio and fit with a model for either one set or two sets of binding sites using the MicroCal Origin version 5.0 software. The calorimeter was calibrated both electronically and chemically as described previously (*25*). The buffer solutions for the ITC experiments contained 10 mM EPPS (pH 7.5), 0.1 mM EDTA, and sufficient NaCl to bring the total Na^+ concentration to 100 mM.

HIV-1 Replication Assay. MT2 cells, a human T cell line ($CD4^+$), were maintained in RPMI 1640 medium supplemented with 10% fetal bovine serum. The MT2 cells were plated in a 96-well plate at 2×10^4 cells (in 150 μL) per well. The cells were infected with HIV-1 LAI strain at a multiplicity of infection (MOI) of 0.01, with control cells being mock-infected with medium. Differing concentrations (ranging from 0 to 8 mM) of neomycin, paromomycin, or ribostamycin were added to the cells immediately following infection. Cells were then cultured at 37 °C for 6 days in a 5% CO_2 incubator. Viral production was assessed by measurement of virion-associated RT activity in culture supernatants. Drug cytotoxicity was measured using previously described (*26*) MTT-based cell viability assays. All experiments were conducted in triplicate.

Virion-associated RT activity was determined using a modification of a previously described protocol (*27*). Both infected and control uninfected cell supernatants were harvested at days 3, 4, 5, and 6. Supernatant (10 μL) was mixed with 50 μL of a solution containing 5 μg/mL poly(rA) template, 0.16 μg/mL oligo$(dT)_{12-18}$ primer, 60 mM Tris (pH 7.8), 75 mM KCl, 5 mM $MgCl_2$, 0.1% Nonidet P-40, 1 mM EDTA, and 10 μCi/mL [α-^{32}P]dTTP (3000 Ci/mmol). After incubation at 37 °C for 90 min, 5 μL of each reaction mixture was spotted onto Whatman DEAE-81 ion-exchange paper and washed four times with 2× saline sodium citrate (SSC) to remove free nucleotides. The paper was subsequently air-dried, subjected to autoradiography at −80 °C with Kodak XAR-5 film, and analyzed using a phosphoimager (Molecular Dynamics, Inc.).

RESULTS AND DISCUSSION

Aminoglycosides Inhibit Specific HIV-1 RT-Mediated RNase H Cleavage of the 18C·18R and 18C·18D Duplexes. Figure 3B (lane 2) shows the RT-induced RNase H cleavage profile of the 18C·18R duplex. Note that RT endonucleolytically cleaves the RNA strand (18R) opposite the chimeric RNA−DNA strand (18C) at three distinct sites (denoted by arrows in Figure 3A,B). The primary cleavage site lies between base positions +1 and +2 (counting from the RNA−DNA junction in the 5′ direction on the cleaved RNA strand). Two other minor cleavage sites lie between positions +3 and +4 and between positions −1 and +1, with the former site being cleaved to a greater extent than the latter site. The Heumann group observed a similar cleavage pattern when probing for HIV-1 RT-mediated RNase H cleavage of a primer binding site (PBS) containing RNA template following RT-mediated DNA polymerization from a tRNA(Lys3) primer hybridized to the RNA template strand (*28*). This concordance between cleavage patterns validates the use of the oligomeric 18C·18R construct studied here as a model for the RT-associated RNase H substrate that follows minus-strand strong-stop DNA synthesis.

Figure 3E (lane 3) shows the RT-induced RNase H cleavage profile of the 18C·18D duplex. When this duplex serves as the substrate, RT cleaves the RNA portion of the chimeric strand (18C) opposite the DNA strand (18D) at only a single site (denoted by the arrow in Figure 3D,E), in

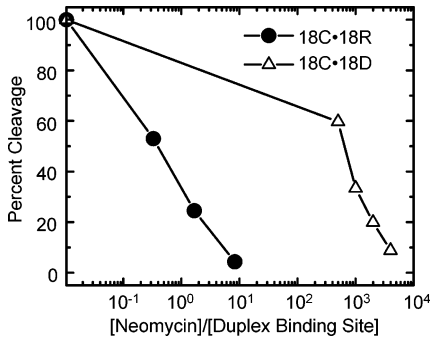

FIGURE 4: The extent of neomycin-induced inhibition of RT-mediated RNase H cleavage depends on drug concentration. Plot depicting the extent of RNase H cleavage as a function of the [neomycin]/[duplex binding site] ratio (r_{bs}) for the 18C•18R (filled circles) and 18C•18D (open triangles) duplexes. For clarity of presentation, the *x*-axis is depicted in a logarithmic scale.

marked contrast to the three cleavage sites observed when the 18C•18R duplex serves as the substrate. This unique cleavage site, which lies between base positions +1 and +2 (counting from the RNA−DNA junction in the 5′ direction on the cleaved chimeric strand), is identical to that observed in previous studies (*29*, *30*), suggesting that the 18C•18D duplex represents a good mimic of the RNase H substrate of RT that follows plus-strand strong-stop synthesis.

Further inspection of Figure 3 reveals that neomycin, paromomycin, and ribostamycin inhibit RT-mediated cleavage of both the 18C•18R (Figure 3B, lanes 3−5) and 18C•18D (Figure 3E, lanes 4−6) duplexes. Furthermore, the extent to which the drugs inhibit cleavage of each of the two duplexes follows the same hierarchy, neomycin > paromomycin > ribostamycin.

Neomycin, Paromomycin, and Ribostamycin Inhibit RT-Mediated RNase H Cleavage of the 18C•18R Duplex with a Greater Efficacy than the 18C•18D Duplex. Panels C and F of Figure 3 present quantitative estimates of the extents of RNase H cleavage for the indicated lanes in panels B and E of Figure 3, respectively. In the presence of the three drugs, the 18C•18D duplex is cleaved to a greater extent than the 18C•18R duplex (8.8% versus 5.1% cleavage in the presence of neomycin, 41.5% versus 18.1% cleavage in the presence of paromomycin, and 84.6% versus 39.1% cleavage in the presence of ribostamycin). Note that a [drug]/[duplex] ratio (r_{dup}) of 4000 was used in the 18C•18D cleavage experiments, compared with a corresponding r_{dup} ratio of only 125 in the 18C•18R experiments. Thus, the greater cleavage of 18C•18D versus 18C•18R occurs despite the presence of 32-fold more aminoglycoside. In the aggregate, these observations indicate that the three aminoglycosides inhibit RT-mediated cleavage of the 18C•18R duplex with a greater efficacy than the 18C•18D duplex. To further quantify this difference in efficacy, we monitored the dependence of aminoglycoside-induced cleavage inhibition on drug concentration. For meaningful comparisons, each drug concentration employed was normalized relative to the total concentration of binding sites to yield a ratio of [drug]/[duplex binding site] (r_{bs}). As detailed below, the drug-to-duplex binding stoichiometries required for these normalizations (3 to 1 for 18C•18R and 1 to 1 for 18C•18D) were determined from ITC measurements. Using neomycin as an illustrative example, Figure 4 graphically depicts the r_{bs} dependence of RT-mediated cleavage of the 18C•18R (filled circles) and 18C•18D (open triangles) duplexes. Note that roughly 1000-fold more neomycin is required to achieve a similar inhibitory effect on RT-mediated cleavage of 18C•18D relative to 18C•18R, with a similar result being obtained for paromomycin (not shown).

Our ITC studies discussed below reveal that both neomycin and paromomycin bind to the 18C•18R duplex with a higher affinity than the 18C•18D duplex. Thus, it is reasonable to suggest that the enhanced efficacy with which both drugs inhibit RT-mediated RNase H cleavage of the 18C•18R duplex relative to the 18C•18D duplex is derived, at least in part, from the differential affinities of the drugs for the two host duplexes. However, the magnitudes of these differential affinities (2-fold in the case of neomycin and 4-fold in the case of paromomycin) do not appear to be sufficient to account for the corresponding 1000-fold differential potency with which the drugs inhibit RT-mediated RNase H cleavage of the 18C•18R and 18C•18D duplexes. Another potential contributing factor to this observed difference in the efficacy of RNase H cleavage inhibition might be derived from the differential number of domains on the two host duplexes that can be targeted by the aminoglycosides. Both 18C•18R and 18C•18D have a nine base pair region of hybrid RNA•DNA, in which RT cleaves the RNA strand. However, the remaining nine base pair region in each of the two duplexes (from positions −1 to −9 in the 18C•18R duplex and from positions +1 to +9 in the 18C•18D duplex) differs with respect to strand composition, being RNA•RNA in the 18C•18R duplex and DNA•DNA in the 18C•18D duplex (compare panels A and D of Figure 3). As noted above, duplex RNA is known to adopt an A-conformation, while duplex DNA adopts a B-conformation (*17*). Recall that 2-DOS aminoglycosides are A-form-specific nucleic acid binding drugs (*13*−*16*). Hence, these drugs can target the RNA•RNA portion of the 18C•18R duplex but not the DNA•DNA portion of the 18C•18D duplex. The differential abilities of neomycin and the +1 to +9 base pair region of paromomycin to target the −1 to −9 base pair region of 18C•18R and 18C•18D may contribute to the differential potency with which each drug inhibits RT-mediated RNase H cleavage of the two duplexes.

Inhibition of RT-Mediated RNase H Cleavage by Neomycin Is Competitive in Nature. To determine the mechanism of aminoglycoside-induced inhibition of RT-mediated RNase H cleavage, we examined the impact of RT concentration on the inhibition of RNase H cleavage induced by neomycin. Figure 5 shows the results of this determination, using the 18C•18D duplex as the RT substrate. Note that, in the presence of neomycin at an r_{bs} ratio of 2000, RT-mediated RNase H cleavage of the 18C strand is inhibited by ≈80%. Further inspection of Figure 5 reveals that this inhibitory effect can be overcome by increasing the amount of RT, an observation indicating that the manner in which neomycin inhibits RT-mediated cleavage of the 18C•18D duplex is *competitive* in nature. This result implies that the extent to which a given concentration of aminoglycoside inhibits RT-mediated RNase H cleavage depends on the nucleic acid binding affinity of not only the drug but also the enzyme. Thus, a third potential factor contributing to the differential efficacy (noted above) with which the aminoglycosides inhibit RT-mediated RNase H cleavage of 18C•18R and 18C•18D may be related to the affinity of RT for the two host

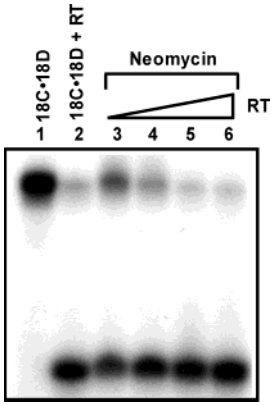

FIGURE 5: Inhibition of RT-mediated RNase H cleavage by neomycin is competitive in nature. Denaturing polyacrylamide gel showing RT-mediated RNase H cleavage of the 18C·18D duplex in the absence or presence of neomycin as a function of RT concentration. The neomycin concentration in lanes 3−6 is 1.0 mM. The amount of RT in lanes 1, 2, 3, 4, 5, and 6 is 0, 0.1, 0.1, 0.3, 0.9, and 2.7 μg, respectively.

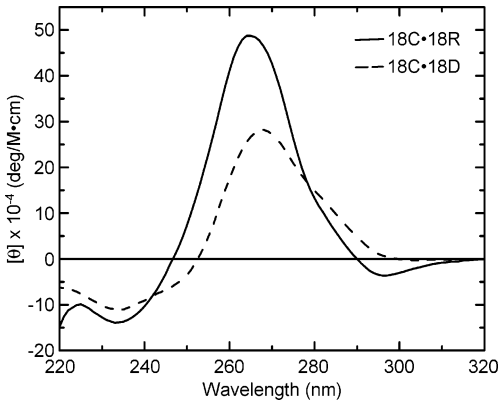

FIGURE 6: CD spectra (at 25 °C) of the 18C·18R (solid line) and 18C·18D (dashed line) duplexes (5 μM) in the absence of drug. Molar ellipticity ([θ]) is expressed in units of deg/(M·cm), where M refers to moles of duplex per liter. The solution conditions were 10 mM sodium cacodylate (pH 6.0), 0.1 mM EDTA, and sufficient NaCl to bring the total Na^+ concentration to 25 mM.

duplexes. In this connection, RT may bind to the 18C·18D duplex with a higher affinity than the 18C·18R duplex, thereby diminishing the inhibitory impact of aminoglycoside binding on RT-mediated cleavage of 18C·18D relative to 18C·18R.

CD Studies Are Consistent with 18C·18R Adopting a More A-like Overall Conformation than 18C·18D. As discussed above, RNA·RNA and DNA·RNA hybrid duplexes adopt A-like conformations, while DNA·DNA duplexes adopt B-like conformations (*17*). Recall that both the 18C·18D and 18C·18R duplexes contain DNA·RNA domains. However, the remaining portion of 18C·18D is DNA·DNA, in contrast to the RNA·RNA domain that is present in the 18C·18R. This difference should result in the 18C·18R duplex adopting a more A-like overall conformation than 18C·18D. In agreement with this prediction, the CD spectrum of the 18C·18R duplex is reflective of a more A-like conformation than that of the 18C·18D duplex, which exhibits signatures characteristic of both A- and B-conformations (Figure 6) (*31*, *32*). Titrations of both 18C·18R and 18C·18D with paromomycin altered their duplex CD spectra in a manner consistent with a shift to more canonical A-conformations

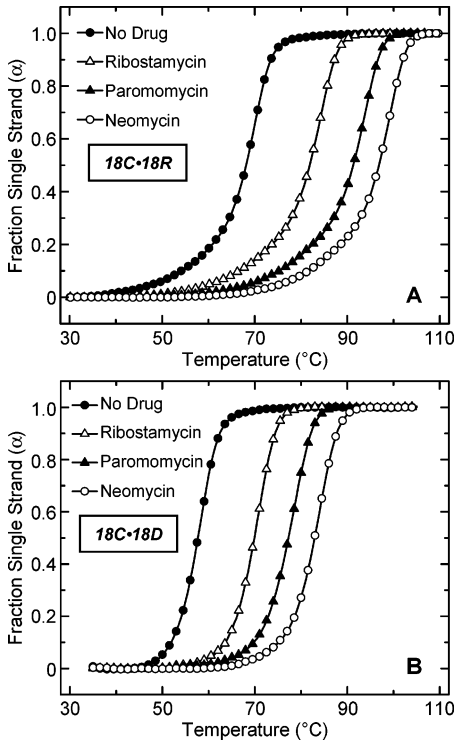

FIGURE 7: UV melting profiles for the 18C·18R (A) and 18C·18D (B) duplexes in the absence (open circles) and presence of neomycin (filled triangles), paromomycin (open squares), and ribostamycin (filled circles). The drug-containing experiments were conducted at a [drug]/[duplex] ratio (r_{dup}) of 5, thereby ensuring the saturation of both duplexes with drug. The duplex concentration was 2 μM, and the solution conditions were as described in the legend to Figure 5. For clarity of presentation, the melting curves were normalized by subtraction of the upper and lower baselines to yield plots of fraction single strand (α) versus temperature (*24*). All of the UV melting profiles were acquired at 274 nm.

Table 1: Impact of Aminoglycoside Binding on the Thermal Stabilities of the 18C·18R and 18C·18D Duplexes[a]

duplex	drug	T_m (°C)
18C·18R	none	68.1
18C·18R	neomycin	96.9
18C·18R	paromomycin	91.3
18C·18R	ribostamycin	81.9
18C·18D	none	57.7
18C·18D	neomycin	82.9
18C·18D	paromomycin	77.3
18C·18D	ribostamycin	69.9

[a] Solution conditions were 10 mM sodium cacodylate (pH 6.0), 0.1 mM EDTA, and sufficient NaCl to bring the total Na^+ concentration to 25 mM. All drug-containing experiments were conducted at a [drug]/[duplex] ratio (r_{dup}) of 5, thereby reflecting conditions where the host duplexes were saturated with drug.

(not shown), an observation highlighting the A-form specific binding properties of aminoglycosides (*13*−*16*).

Neomycin, Paromomycin, and Ribostamycin Bind to and Enhance the Thermal Stabilities of the 18C·18R and 18C·18D Duplexes. Figure 7 shows the UV melting curves for the 18C·18R and 18C·18D duplexes in the absence and presence of saturating concentrations of neomycin, paromomycin, or ribostamycin. The melting temperatures (T_m) derived from these thermal denaturation profiles are summarized in Table 1. Note that the presence of either aminoglycoside enhances the thermal stability of each target duplex, an observation consistent with the aminoglycosides

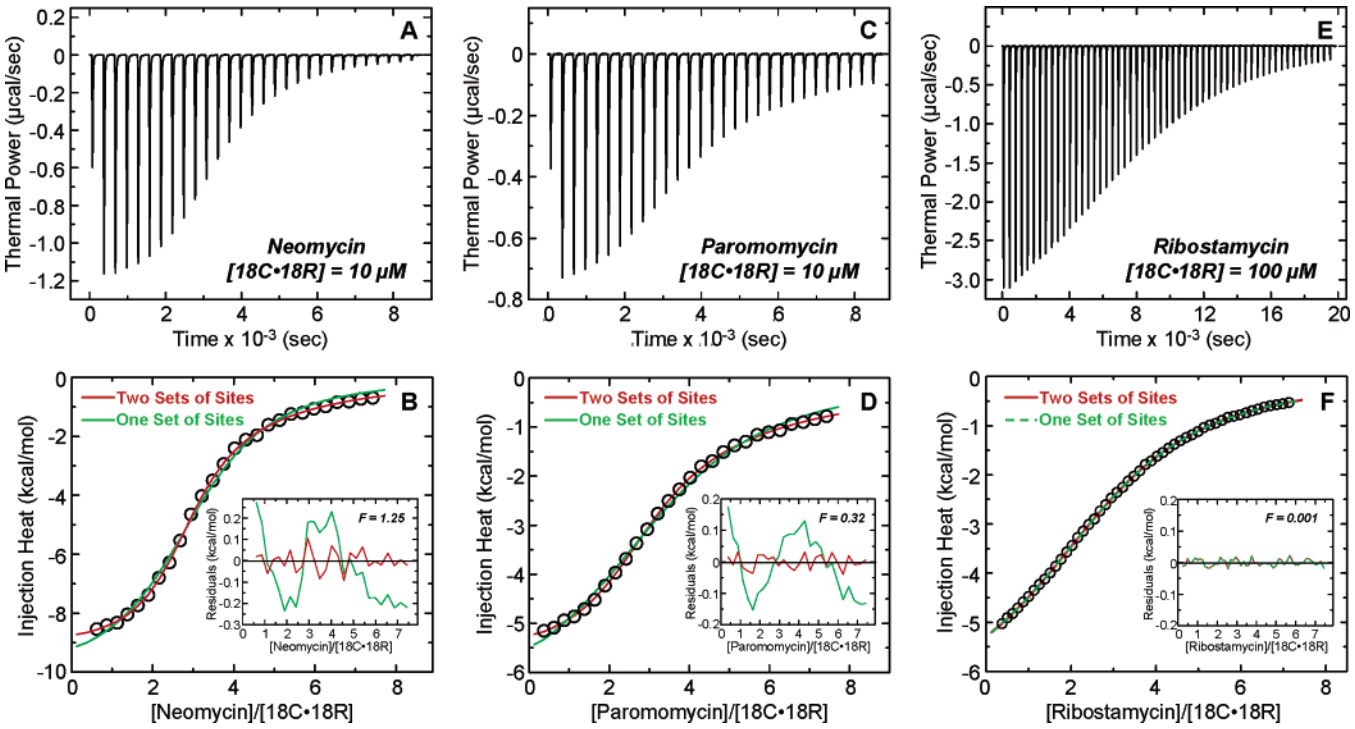

FIGURE 8: ITC profiles at 25 °C for the titration of neomycin (A, B), paromomycin (C, D), and ribostamycin (E, F) into a solution containing the 18C·18R duplex at the indicated concentration. Each heat burst curve is the result of an injection of a drug solution that was 35-fold more concentrated than the duplex solution. Panels B, D, and F show the corrected injection heats plotted as a function of the [drug]/[18C·18R] ratio. These heats were derived by integration of the ITC profiles shown in panels A, C, and E followed by subtraction of the corresponding dilution heats derived from control titrations of drug into buffer alone. The data points in panels B, D, and F reflect the corrected experimental injection heats, while the lines reflect calculated fits of the data with models for either one set of binding sites (green) or two sets of binding sites (red). The insets in panels B, D, and F show the residuals of the fitted lines relative to the experimental data points. The residuals were analyzed with a one-way ANOVA test to yield the indicated *F* statistics. This analysis revealed that the neomycin and paromomycin data (panels B and D, respectively) were best fit by a model for two sets of binding sites, while the ribostamycin data (panel F) were fit equally well by a model for one set or two sets of binding sites. The solution conditions were 10 mM EPPS (pH 7.5), 0.1 mM EDTA, and sufficient NaCl to bring the total Na^+ concentration to 100 mM.

binding to the two host duplexes with a preference for the duplex versus the single-stranded state. When 18C·18R serves as the host duplex, the binding of neomycin, paromomycin, and ribostamycin enhances the thermal stability (i.e., T_m) of the duplex by 28.8, 23.2, and 13.8 °C, respectively (Figure 7A). When 18C·18D serves as the host duplex, the corresponding ΔT_m values are 25.2, 19.6, and 12.2 °C (Figure 7B). Thus, the extent of drug-induced enhancement in the thermal stabilities of both target duplexes follows the hierarchy neomycin > paromomycin > ribostamycin. Note the consistency between this ΔT_m-based hierarchy and that described above for inhibition of RT-mediated RNase cleavage.

Further inspection of the data in Table 1 reveals that the binding of all three drugs enhances the thermal stability of the 18C·18R duplex to a greater extent than the 18C·18D duplex. In other words, as measured by differences in ΔT_m ($\Delta\Delta T_m$), the three drugs are able to distinguish between the two duplex targets, which differ with respect to their strand composition (RNA versus DNA). It is likely that the basis for this discrimination lies in an enhanced propensity for the 18C·18R to adopt an overall A-like conformation relative to 18C·18D (Figure 6), which, unlike 18C·18R, contains a DNA·DNA domain.

Note that the ΔT_m data described above are related to drug−duplex binding affinity in a manner that depends on the binding enthalpy and the binding stoichiometry, as well as the transition enthalpy for the melting of the host duplex (*33*, *34*). Thus, differences in ΔT_m are not necessarily correlated with differences in binding affinity. In the section that follows, we describe how ITC can be used to determine drug−duplex binding affinities and stoichiometries.

The Relative Binding Affinities of Neomycin, Paromomycin, and Ribostamycin for 18C·18R and 18C·18D Correlate with the Relative Extents to Which the Drugs Thermally Stabilize and Inhibit RT-Mediated RNase H Cleavage of the Two Host Duplexes. We used ITC to characterize the binding of neomycin, paromomycin, and ribostamycin to the 18C·18R and 18C·18D duplexes at 25 °C. Figure 8 shows the ITC profiles resulting from injection of neomycin (Figure 8A), paromomycin (Figure 8C), or ribostamycin (Figure 8E) into a solution of 18C·18R. The corresponding ITC profiles resulting from injection of the three drugs into a solution of 18C·18D are shown in panels A, C, and E of Figure 9. Each of the heat burst curves in panels A, C, and E of Figures 8 and 9 corresponds to a single drug injection. The areas under these heat burst curves were determined by integration to yield the associated injection heats. These injection heats were corrected by subtraction of the corresponding dilution heats derived from the injection of identical amounts of drug into buffer alone. Panels B, D, and F of Figures 8 and 9 show the corrected injection heats for the titration of the three drugs into the 18C·18R (Figure 8B,D,F) and 18C·18D (Figure 9B,D,F) duplexes plotted as a function of the [drug]/[duplex] ratio. In these six panels, the data points reflect the corrected experimental injection heats, while the lines reflect

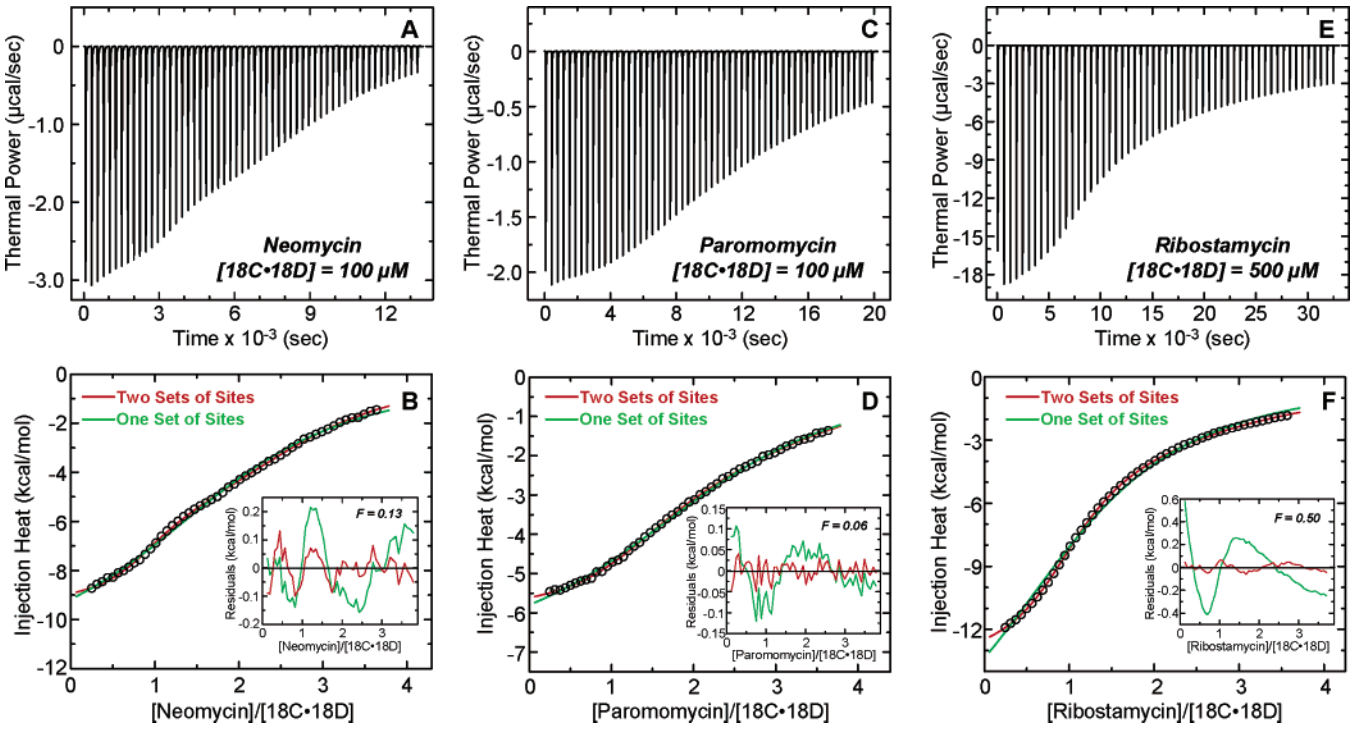

FIGURE 9: ITC profiles at 25 °C for the titration of neomycin (A, B), paromomycin (C, D), and ribostamycin (E, F) into a solution containing the 18C·18D duplex at the indicated concentration. Each heat burst curve is the result of an injection of a drug solution that was 17.5-fold more concentrated than the duplex solution. Panels B, D, and F show the corrected injection heats plotted as a function of the [drug]/[18C·18D] ratio. These heats were derived by integration of the ITC profiles shown in panels A, C, and E followed by subtraction of the corresponding dilution heats derived from control titrations of drug into buffer alone. The data points in panels B, D, and F reflect the corrected experimental injection heats, while the solid lines reflect calculated fits of the data with models for either one set of binding sites (green) or two sets of binding sites (red). The insets in panels B, D, and F show the residuals of the fitted lines relative to the experimental data points. The residuals were analyzed with a one-way ANOVA test to yield the indicated *F* statistics. This analysis revealed that each of the injection heat profiles was best fit by a model for two sets of binding sites. The solution conditions were as described in the legend to Figure 8.

Table 2: ITC-Derived Binding Parameters for the Complexation of Neomycin, Paromomycin, and Ribostamycin with the 18C·18R and 18C·18D Duplexes at 25 °C[a]

duplex	drug	N_1[b]	K_1[c] (M^{-1})	ΔH_1[c] (kcal/mol)	N_2[b]	K_2[c] (M^{-1})	ΔH_2[c] (kcal/mol)
18C·18R	neomycin	2.7 ± 0.1	$(1.1 \pm 0.3) \times 10^6$	-9.1 ± 0.1	2.0	$(3.5 \pm 1.9) \times 10^4$	-4.9 ± 0.5
18C·18R	paromomycin	2.8 ± 0.2	$(4.2 \pm 1.0) \times 10^5$	-5.6 ± 0.1	2.0	$(1.7 \pm 0.9) \times 10^4$	-6.7 ± 0.9
18C·18R	ribostamycin	3.0 ± 0.1	$(1.1 \pm 0.1) \times 10^4$	-6.8 ± 0.1	NA	NA	NA
18C·18D	neomycin	0.9 ± 0.1	$(5.3 \pm 1.2) \times 10^5$	-9.3 ± 0.1	1.9	$(2.6 \pm 0.1) \times 10^4$	-6.7 ± 0.3
18C·18D	paromomycin	1.3 ± 0.1	$(1.8 \pm 0.3) \times 10^5$	-6.0 ± 0.1	2.0	$(1.3 \pm 0.1) \times 10^4$	-4.4 ± 0.2
18C·18D	ribostamycin	1.0 ± 0.1	$(3.5 \pm 0.4) \times 10^4$	-13.6 ± 0.1	2.0	$(1.6 \pm 0.2) \times 10^3$	-7.2 ± 0.2

[a] Solution conditions were 10 mM EPPS (pH 7.5), 0.1 mM EDTA, and sufficient NaCl to bring the total Na^+ concentration to 100 mM. The binding parameters were derived from best fits of the ITC profiles shown in Figures 8 and 9. A model for two sets of binding sites best fit all of the ITC profiles, except that for the ribostamycin−18C·18R interaction, which was fit equally well by a model for one set or two sets of binding sites. In this latter case, the binding parameters derived from the fit with a model for one set of binding sites are presented, since the additional parameters invoked by the model for two sets of binding sites did not significantly improve the fit (NA denotes not applicable). [b] *N* denotes the drug to duplex binding stoichiometry for each set of binding sites that was fit. The value of N_1 was allowed to vary during the fitting routines, with the indicated uncertainties reflecting the 95% confidence intervals. When invoked, the value of N_2 was fixed during the fitting routine and manually varied to yield the best fit (as reflected by minimization of χ^2). [c] The values of K_1 and ΔH_1 and, when invoked, K_2 and ΔH_2 were allowed to vary during the fitting routines. The indicated uncertainties in these values reflect the 95% confidence intervals.

calculated fits of the data with a model for either one set (green) or two sets (red) of binding sites. A one-way ANOVA analysis of the residuals of the fitted lines relative to the experimental injection heats (see insets to panels B, D, and F of Figures 8 and 9) revealed that all of the ITC profiles were best fit by a model for two sets of binding sites, with the exception of the ribostamycin−18C·18R profile, which was fit equally well by a model for one set or two sets of binding sites. For the acquisition of the fits using the model for two sets of binding sites, the drug−duplex association constants (K_1, K_2), the observed binding enthalpies (ΔH_1, ΔH_2), and the drug−duplex stoichiometry for the first binding event (N_1) were used as free-floating parameters. N_2 was fixed during these fitting routines and manually varied to yield the best fit (as judged by a minimization of χ^2). K_1, ΔH_1, and N_1 were allowed to vary during derivation of the fit using the model for one set of binding sites. The binding parameters derived from the best fits of the ITC data shown in Figures 8 and 9 are summarized in Table 2. In the case of the ribostamycin−18C·18R data set, the relevant binding parameters were derived from the fit with a model for one set of binding sites, since the additional parameters invoked

by the model for two sets of binding sites did not significantly improve the fit. Inspection of the data in Table 2 reveals the following significant features:

(i) In all cases where two sets of binding sites were observed (i.e., for all of the data sets except the ribostamycin−18C·18R data set), drug affinity for the first set of binding sites (K_1) is at least 14-fold greater than that for the second set of binding sites (K_2). We ascribe the "high-affinity" binding sites to specific drug−duplex interactions, which, based on the existing database of aminoglycoside−nucleic acid structures, are likely directed to the duplex major groove. The "low-affinity" binding sites may reflect nonspecific electrostatically driven interactions with phosphate moieties on the host duplex.

(ii) The K_1 values for drug binding to each of the two host duplexes follow the hierarchy neomycin > paromomycin > ribostamycin. Thus, the concordance between the hierarchies of duplex thermal enhancement and RNase H cleavage inhibition noted above also extends to drug−duplex binding affinity. Note that, when either 18C·18R or 18C·18D serves as the target duplex, the differences in duplex affinity exhibited by the three drugs are in reasonable quantitative agreement with the corresponding differences in the extents of RNase H cleavage inhibition.

(iii) N_1 for drug binding to the 18C·18R duplex (approximately 3 drug molecules per duplex) is greater than for drug binding to the 18C·18D duplex (approximately 1 drug molecule per duplex). Recall that aminoglycosides can target RNA·RNA and DNA·RNA duplex domains but not DNA·DNA duplex domains. Thus, both the DNA·RNA and RNA·RNA portions of the 18C·18R duplex are potential binding sites for aminoglycosides. By contrast, only the RNA·DNA portion of the 18C·18D duplex can serve as a target for aminoglycoside binding, thereby accounting for the larger value of N_1 when 18C·18R serves as the host duplex.

(iv) Neomycin and paromomycin exhibit higher affinities (as reflected by values of K_1) for the 18C·18R duplex than for the 18C·18D duplex. We have previously shown that aminoglycosides bind to RNA·RNA duplexes with a higher affinity than to the corresponding RNA·DNA hybrid duplexes, due, at least in part, to the former duplexes adopting more canonical A-conformations than the latter duplexes (*13*). Recall that the 18C·18R duplex contains an RNA·RNA region that is lacking in the 18C·18D duplex. Furthermore, a recently reported crystal structure of the r(gcca)-d(CTGC)·r(gcaguggc) chimeric duplex, which comprises the eight central base pairs of the 18C·18R duplex, revealed no significant differences in A-like helix geometry between the RNA·RNA and RNA·DNA halves of the duplex (*18*). These observations, coupled with our CD results discussed above, suggest that the enhanced affinity of neomycin and paromomycin for 18C·18R relative to 18C·18D is a consequence of the former duplex adopting a more A-like conformation than the latter duplex.

The Correlation between Relative Duplex Binding Affinity and Relative Inhibition of RT-Mediated RNase H Cleavage Also Extends to Relative Inhibition of HIV-1 Replication. We monitored the impact of neomycin, paromomycin, and ribostamycin on HIV-1 replication in MT2 cells using a virion-associated RT activity assay. Neomycin treatment results in a dose-dependent decrease in supernatant HIV RT activity (indicative of virus production) over a 6 day time course postinfection (Figure 10A). The antiviral activities of all three drugs (as determined by virion RT production at day 6) are shown in Figure 10B,C. Neomycin induced the most potent inhibition of RT activity, yielding inhibition percentages of approximately 89% and 99% at concentrations of 2 and 4 mM, respectively. At these same two concentrations, paromomycin inhibited RT activity by approximately 54% and 94%, with ribostamycin inhibiting viral production by only 43% at the highest dose of 8 mM. Note the consistency between this hierarchy of antiviral activity and the corresponding hierarchies described above for the inhibition of RT-mediated RNase H cleavage, duplex thermal enhancement, and duplex binding affinity. This consistency highlights the possibility that the antiviral activities of the

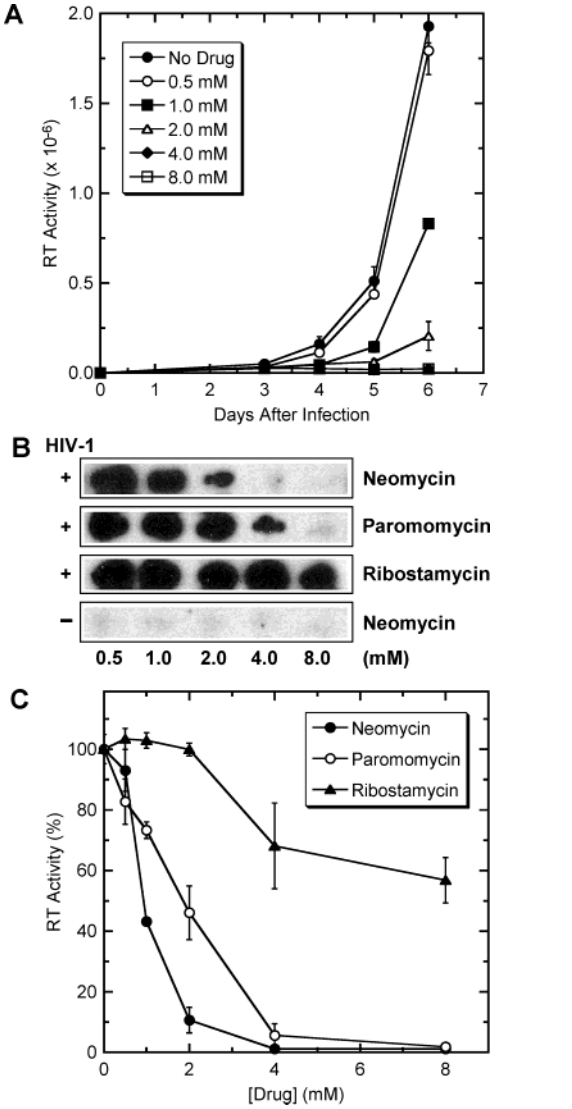

FIGURE 10: Inhibition of HIV-1 viral production (as measured using the RT assay described in Materials and Methods) in MT2 cells by neomycin, paromomycin, and ribostamycin. (A) Kinetics of viral growth following treatment with the indicated concentrations of neomycin. (B) Aminoglycoside-induced inhibition of viral replication 6 days after infection. The identities of the aminoglycosides and their concentrations are as indicated. The plus sign denotes infected cells, while the minus sign denotes uninfected cells. (C) Quantitation of the autoradiogram shown in panel B. The data points in panels A and C reflect averages from three independent experiments, with the error bars reflecting standard deviations from the mean.

Table 3: Antiviral and Cytotoxic Activities of the Aminoglycosides

drug	viral inhibition[a]	cytotoxicity[a]
neomycin	0.9	>8.0
paromomycin	1.8	3.4
ribostamycin	>8.0	>8.0

[a] The indicated values are IC_{50} values, which, for viral inhibition, represent the drug concentrations (in mM) at which viral production (as measured by RT assay) is inhibited by 50%. For cytotoxicity, the indicated IC_{50} values reflect the drug concentrations (in mM) that induce 50% cell death, as measured by MTT assay.

aminoglycosides may be due, at least in part, to drug targeting of viral RNA·DNA hybrid structures and subsequent interference with RT-mediated RNase H activity.

An important issue when considering the antiviral activities noted above is the relative cytotoxicities of the three drugs. As shown in Table 3, the IC_{50} of neomycin for HIV replication was 0.9 mM, compared with a corresponding IC_{50} for cytotoxicity of >8.0 mM. This differential in neomycin IC_{50} values for viral replication and cytotoxicity translates to a therapeutic index of at least 9-fold. By contrast, paromomycin and ribostamycin failed to show significant inhibition of HIV replication at noncytotoxic levels (with the IC_{50} values for viral replication and cytotoxicity being 1.8 and 3.4 mM for paromomycin and >8.0 mM for ribostamycin).

Neomycin has been shown to inhibit HIV-1 production in infected U1 monocytes (*35*) and $CD4^+$ HeLa cells (*36*), with tobramycin also having been found to inhibit viral production in the latter cells (*36*). The basis for these antiviral activities has been attributed to the abilities of the aminoglycosides to antagonize the interactions between viral proteins and their specific RNA substrates [e.g., the interactions between Rev and the Rev response element (RRE) as well as between Tat and the Tat activating region (TAR)] (*35*−*43*). These RNA substrates, as well as the RNA−DNA chimeric substrates discussed in this report, all represent potential targets that underlie the observed anti-HIV-1 activities of aminoglycosides. In support of this possibility, our recent ITC studies have revealed that, under similar solution conditions, the affinities of neomycin and paromomycin for the RRE are similar in magnitude to those they exhibit for the RNA−DNA chimeric structures studied here (unpublished results). It is interesting to note that the processing of the RNA·DNA substrates studied here via the RNase H activity of RT occurs earlier in the postinfection HIV-1 life cycle than the interactions of Tat and Rev with their cognate RNA targets (*44*). However, the therapeutic significance of this difference remains to be assessed.

CONCLUDING REMARKS

Using the aminoglycosides neomycin, paromomycin, and ribostamycin as model ligands, we have described an approach for inhibiting HIV-1 RT-mediated RNase H activity by targeting the RNA−DNA chimeric structures that serve as the normal substrates for this enzymatic activity, which is an essential component of viral replication (*4*, *5*). Significantly, such an approach should not be compromised by the genetic diversity of the virus. We show that, with regard to RNase H cleavage inhibition, duplex binding affinity, and antiviral activity, the three aminoglycosides follow a similar hierarchy of neomycin > paromomycin > ribostamycin. One of the key differences between the three drugs is the number of amino groups each drug possesses, with neomycin, paromomycin, and ribostamycin having 6, 5, and 4 amino groups, respectively (see Figure 2). Thus, the hierarchy noted above suggests that the number of drug amino groups may be an important determinant in the duplex binding, RNase H inhibitory, and antiviral properties of the drugs. We have previously demonstrated that aminoglycoside binding to various RNA and RNA·DNA hybrid duplexes is coupled to protonation of one or more drug amino groups (*13*, *45*), an observation highlighting the importance of not only the number of amino groups in aminoglycoside recognition of these nucleic acid structural domains but also that the amino groups be in their protonated cationic (NH_3^+) states. Thus, modifications that promote or preserve the cationic state of the drug amino groups at physiological values of pH should enhance nucleic acid affinity, RNase H cleavage inhibition, and, ultimately, antiviral activity. Such drug modifications might include dehydroxylation of positions (e.g., the 3″-, 3′-, and 6-positions) adjacent to amino groups, thereby raising the pK_a values of the adjacent amino groups. Conversion of specific amino groups (e.g., the 2′- and 3-amino groups) to alkylamines would also serve to raise the pH range over which the amino functionalities would exist in their NH_3^+ states.

The drug modifications discussed above address the issue of drug affinity for the nucleic acid target. However, it is also important to consider the issue of drug specificity. In addition to binding RNA−DNA hybrid duplexes, aminoglycosides also bind to other nucleic acid structures that adopt A-like conformations, including DNA and RNA triplexes, duplex RNA, and certain duplex DNA sequences (*12*−*16*, *45*, *46*). It is likely that improving drug specificity for the nucleic acid substrates of the RNase H activity of RT will result in enhanced antiviral activity as well as reduced host cellular toxicity. In this connection, recent crystallographic and NMR studies on octameric oligonucleotide duplexes that model the same two RNase H substrates of RT mimicked by the 18mer duplexes used in the studies presented here reveal that these duplexes exhibit some unusual structural properties that are dictated, at least in part, by the presence of RNA−DNA junctions (*18*, *19*). In fact, the unusual structural properties associated with the presence of RNA−DNA junctions are thought to be determining factors in the specificity of RT-mediated RNase H cleavage (*18*, *19*). The current structural database offers the opportunity of using computational methods to identify and develop aminoglycoside-based and other novel compounds that target these unusual structural motifs with a high degree of affinity and specificity.

ACKNOWLEDGMENT

The $pKKRT_{66}HH$ plasmid was the generous gift of Dr. V. N. Pandey. We thank Dr. Malvika Kaul for helpful discussions and critical reading of the manuscript.

REFERENCES

1. Telesnitsky, A., and Goff, S. P. (1997) in *Retroviruses* (Coffin, J. M., Hughes, S. H., and Varmus, H. E., Eds.) pp 121−160, Cold Spring Harbor Laboratory Press, New York.
2. Larder, B. A. (1993) in *Reverse Transcriptase* (Skalka, A. M., and Goff, S. P., Eds.) pp 205−222, Cold Spring Harbor Laboratory Press, New York.

3. Richman, D. D. (2001) HIV Chemotherapy, *Nature 410*, 995−1001.
4. Schatz, O., Cromme, F., Naas, T., Lindemann, D., Mous, J., and Le Grice, S. F. J. (1990) in *Oncogenesis and AIDS* (Papas, T., Ed.) pp 304−315, Portfolio Publishing, Woodlands, TX.
5. Tisdale, M., Schulze, T., Larder, B. A., and Moelling, K. (1991) Mutations within the RNase H Domain of HIV-1 Reverse Transcriptase Abolish Viral Infectivity, *J. Gen. Virol. 72*, 59−66.
6. Champoux, J. J. (1993) in *Reverse Transcriptase* (Skalka, A. M., and Goff, S. P., Eds.) pp 103−117, Cold Spring Harbor Laboratory Press, New York.
7. Nabel, G. J. (2001) Challenges and Opportunities for Development of an AIDS Vaccine, *Nature 410*, 1002−1007.
8. Root, M. J., Kay, M. S., and Kim, P. S. (2001) Protein Design of an HIV-1 Entry Inhibitor, *Science 291*, 884−888.
9. Lalezari, J. P., Henry, K., O'Hearn, M., Montaner, J. S., Piliero, P. J., Trottier, B., Walmsley, S., Cohen, C., Kuritzkes, D. R., Eron, J. J., Jr., Chung, J., DeMasi, R., Donatacci, L., Drobnes, C., Delehanty, J., and Salgo, M. (2003) Enfuvirtide, an HIV-1 Fusion Inhibitor, for Drug-Resistant HIV Infection in North and South America, *N. Engl. J. Med. 348*, 2175−2185.
10. Cervia, J. S., and Smith, M. A. (2003) Enfuvirtide (T-20): A Novel Human Immunodeficiency Virus Type 1 Fusion Inhibitor, *Clin. Infect. Dis. 37*, 1102−1106.
11. Ren, J., Qu, X., Dattagupta, N., and Chaires, J. B. (2001) Molecular Recognition of a RNA:DNA Hybrid Structure, *J. Am. Chem. Soc. 123*, 6742−6743.
12. Arya, D. P., Coffee, R. L., Jr., and Charles, I. (2001) Neomycin-Induced Hybrid Triplex Formation, *J. Am. Chem. Soc. 123*, 11093−11094.
13. Barbieri, C. M., Li, T.-K., Guo, S., Wang, G., Shallop, A. J., Pan, W., Yang, G., Gaffney, B. L., Jones, R. A., and Pilch, D. S. (2003) Aminoglycoside Complexation with a DNA·RNA Hybrid Duplex: The Thermodynamics of Recognition and Inhibition of RNA Processing Enzymes, *J. Am. Chem. Soc. 125*, 6469−6477.
14. Robinson, H., and Wang, A. H.-J. (1996) Neomycin, Spermine and Hexaamminecobalt(III) Share Common Structural Motifs in Converting B- to A-DNA, *Nucleic Acids Res. 24*, 676−682.
15. Chen, Q., Shafer, R. H., and Kuntz, I. D. (1997) Structure-Based Discovery of Ligands Targeted to the RNA Double Helix, *Biochemistry 36*, 11402−11407.
16. Arya, D. P., Xue, L., and Willis, B. (2003) Aminoglycoside (Neomycin) Preference is for A-form Nucleic Acids, not Just RNA: Results from a Competition Dialysis Study, *J. Am. Chem. Soc. 125*, 10148−10149.
17. Saenger, W. (1983) *Principles of Nucleic Acid Structure*, Springer-Verlag, New York.
18. Mueller, U., Maier, G., Onori, A. M., Cellai, L., Heumann, H., and Heinemann, U. (1998) Crystal Structure of an Eight-Base Pair Duplex Containing the 3′-DNA-RNA-5′ Junction Formed During Initiation of Minus-Strand Synthesis of HIV Replication, *Biochemistry 37*, 12005−12011.
19. Fedoroff, O. Y., Salazar, M., and Reid, B. R. (1996) Structural Variation Among Retroviral Primer-DNA Junctions: Solution Structure of the HIV-1 (−)-Strand Okazaki Fragment r(gcca)d(CTGC)·d(GCAGTGGC), *Biochemistry 35*, 11070−11080.
20. Beard, W. A., and Wilson, S. H. (1993) Kinetic Analysis of Template·Primer Interactions with Recombinant Forms of HIV-1 Reverse Transcriptase, *Biochemistry 32*, 9745−9753.
21. Pandey, V. N., Kaushik, N., Rege, N., Sarafianos, S. G., Yadav, P. N. S., and Modak, M. J. (1996) Role of Methionine 184 of Human Immunodeficiency Virus Type-1 Reverse Transcriptase in the Polymerase Function and Fidelity of DNA Synthesis, *Biochemistry 35*, 2168−2179.
22. Song, Q., Wang, W., Fischer, A., Zhang, X., Gaffney, B. L., and Jones, R. A. (1999) High Yield Protection of Purine Ribonucleosides for Phosphoramidite RNA Synthesis, *Tetrahedron Lett. 40*, 4153−4156.
23. Song, Q., and Jones, R. A. (1999) Use of Silyl Ethers as Fluoride Scavengers in RNA Synthesis, *Tetrahedron Lett. 40*, 4653−4654.
24. Marky, L. A., and Breslauer, K. J. (1987) Calculating Thermodynamic Data for Transitions of Any Molecularity From Equilibrium Melting Curves, *Biopolymers 26*, 1601−1620.
25. Pilch, D. S., Kirolos, M. A., Liu, X., Plum, G. E., and Breslauer, K. J. (1995) Berenil [1,3-Bis-(4′-amidinophenyl)triazene] Binding to DNA Duplexes and to a RNA Duplex: Evidence for Both Intercalative and Minor Groove Binding Properties, *Biochemistry 34*, 9962−9976.
26. Mosmann, T. (1983) Rapid colorometric Assay for Cellular Growth and Survival: Application to Proliferation and Cytotoxicity Assays, *J. Immunol. Methods 65*, 55−63.
27. Willey, R. L., Smith, D. H., Lasky, L. A., Theodore, T. S., Earl, P. L., Moss, B., Capon, D. J., and Martin, M. A. (1988) *In Vitro* Mutagenesis Identifies a Region within the Envelope Gene of the Human Immunodeficiency Virus that is Critical for Infectivity, *J. Virol. 62*, 139−147.
28. Götte, M., Fackler, S., Hermann, T., Perola, E., Cellai, L., Gross, H. J., Le Grice, S. F. J., and Heumann, H. (1995) HIV-1 Reverse Transcriptase-Associated RNase H Cleaves RNA/RNA in Arrested Complexes: Implications for the Mechanism by which RNase H Discriminates between RNA/RNA and RNA/DNA, *EMBO J. 14*, 833−841.
29. Furfine, E. S., and Reardon, J. E. (1991) Human Immunodeficiency Virus Reverse Transcriptase Ribonuclease H: Specificity of tRNA(Lys3)-Primer Excision, *Biochemistry 30*, 7041−7046.
30. Smith, J. S., and Roth, M. J. (1992) Specificity of Human Immunodeficiency Virus-1 Reverse Transcriptase-Associated Ribonuclease H in Removal of the Minus-Strand Primer, tRNA-(Lys3), *J. Biol. Chem. 267*, 15071−15079.
31. Gray, D. M., and Ratliff, R. L. (1975) Circular Dichroism Spectra of Poly[d(AC):d(GT)], Poly[r(AC):r(GU)], and Hybrids Poly-[d(AC):r(GU)] and Poly[r(AC):d(GT)] in the Presence of Ethanol, *Biopolymers 14*, 487−498.
32. Gray, D. M., Ratliff, R. L., and Vaughan, M. R. (1992) Circular Dichroism Spectroscopy of DNA, *Methods Enzymol. 211*, 389−406.
33. Crothers, D. M. (1971) Statistical Thermodynamics of Nucleic Acid Melting Transitions with Coupled Binding Equilibria, *Biopolymers 10*, 2147−2160.
34. McGhee, J. D. (1976) Theoretical Calculations of the Helix-Coil Transition of DNA in the Presence of Large, Cooperatively Binding Ligands, *Biopolymers 15*, 1345−1375.
35. Zapp, M. L., Stern, S., and Green, M. R. (1993) Small Molecules that Selectively Block RNA Binding of HIV-1 Rev Protein Inhibit Rev Function and Viral Production, *Cell 74*, 969−978.
36. Baker, T. J., Luedtke, N. W., Tor, Y., and Goodman, M. (2000) Synthesis and Anti-HIV Activity of Guanidinoglycosides, *J. Org. Chem. 65*, 9054−9058.
37. Michael, K., and Tor, Y. (1998) Designing Novel RNA Binders, *Chem. Eur. J. 4*, 2091−2098.
38. Wang, S., Huber, P. W., Cui, M., Czarnik, A. W., and Mei, H.-Y. (1998) Binding of Neomycin to the TAR Element of HIV-1 RNA Induces Dissociation of the Tat Protein by an Allosteric Mechanism, *Biochemistry 37*, 5549−5557.
39. Hamy, F., Brondani, V., Flörsheimer, A., Stark, W., Blommers, M. J. J., and Klimkait, T. (1998) A New Class of HIV-1 Tat Antagonist Acting Through Tat-TAR Inhibition, *Biochemistry 37*, 5086−5095.
40. Mei, H.-Y., Cui, M., Heldsinger, A., Lemrow, S. M., Loo, J. A., Sannes-Lowry, K. A., Sharmeen, L., and Czarnik, A. W. (1998) Inhibitors of Protein-RNA Complexation That Target the RNA: Specific Recognition of Human Immunodeficiency Virus Type I TAR RNA by Small Organic Molecules, *Biochemistry 37*, 14204−14212.
41. Tor, Y. (1999) RNA and the Small Molecule World, *Angew. Chem., Int. Ed. Engl. 38*, 1579−1582.
42. Kirk, S. R., Luedtke, N. W., and Tor, Y. (2000) Neomycin-Acridine Conjugate: A Potent Inhibitor of Rev-RRE Binding, *J. Am. Chem. Soc. 122*, 980−981.
43. Luedtke, N. W., Liu, Q., and Tor, Y. (2003) RNA-Ligand Interactions: Affinity and Specificity of Aminoglycoside Dimers and Acriding Conjugates to the HIV-1 Rev Response Element, *Biochemistry 42*, 11391−11403.
44. Tang, H., Kuhen, K. L., and Wong-Staal, F. (1999) Lentivirus Replication and Regulation, *Annu. Rev. Genet. 33*, 133−170.
45. Jin, E., Katritich, V., Olson, W. K., Kharatisvili, M., Abagyan, R., and Pilch, D. S. (2000) Aminoglycoside Binding in the Major Groove of Duplex RNA: The Thermodynamic and Electrostatic Forces That Govern Recognition, *J. Mol. Biol. 298*, 95−110.
46. Arya, D. P., Coffee, R. L., Jr., Willis, B., and Abramovitch, A. I. (2001) Aminoglycoside-Nucleic Acid Interactions: Remarkable Stabilization of DNA and RNA Triple Helicies by Neomycin, *J. Am. Chem. Soc. 123*, 5385−5395.

BI0497345